ORIGINAL PAPER

Hydrated magnesium (II) with H-bonded hexamethylenetetramine and co-ligands: synthesis, structural characterization, thermal decomposition, and hirshfeld surface analysis

Tambua Neville Milo[1] · Che Dieudonne Tabong[2] · Jean Hubert Nono[3] · Eni Donatus Bekindaka[4] ·
Divine Mbom Yufanyi[5] · Moise Ondoh Agwara[6]

Abstract

The reaction of magnesium nitrate with hexamethylenetetramine (HMTA) in the presence of thiocyanide, dicyanamide (DCA), or azide ions resulted in the formation of the hydrated magnesium(II) compounds $[Mg(H_2O)_6](SCN)_2 \cdot 2HMTA \cdot 3H_2O$ (**1a**), $[Mg(H_2O)_6](DCA)_2 \cdot 3HMTA \cdot H_2O$ (**1b**) and $[Mg(H_2O)_6](N_3)_2 \cdot 2HMTA \cdot 4H_2O$ (**1c**) (DCA = dicyanamide). The compounds were characterized by elemental analysis, IR spectroscopy, thermal analysis, and single-crystal X-ray structure analysis. These coordination compounds crystallize in the Triclinic, $P1$, Tetragonal, $P4_2/n$, and Monoclinic, $P2_1/n$ space groups, respectively for **1a**, **1b,** and **1c**. The 3D crystal packing structure results from a combination of O–H/H–N interactions. Hirshfeld surface (HS) analysis of the complexes was undertaken to investigate further the intermolecular interactions. Thermal studies of **1a** and **1b** was undertaken to determine their suitability as precursors for MgO nanoparticles.

Graphical abstract
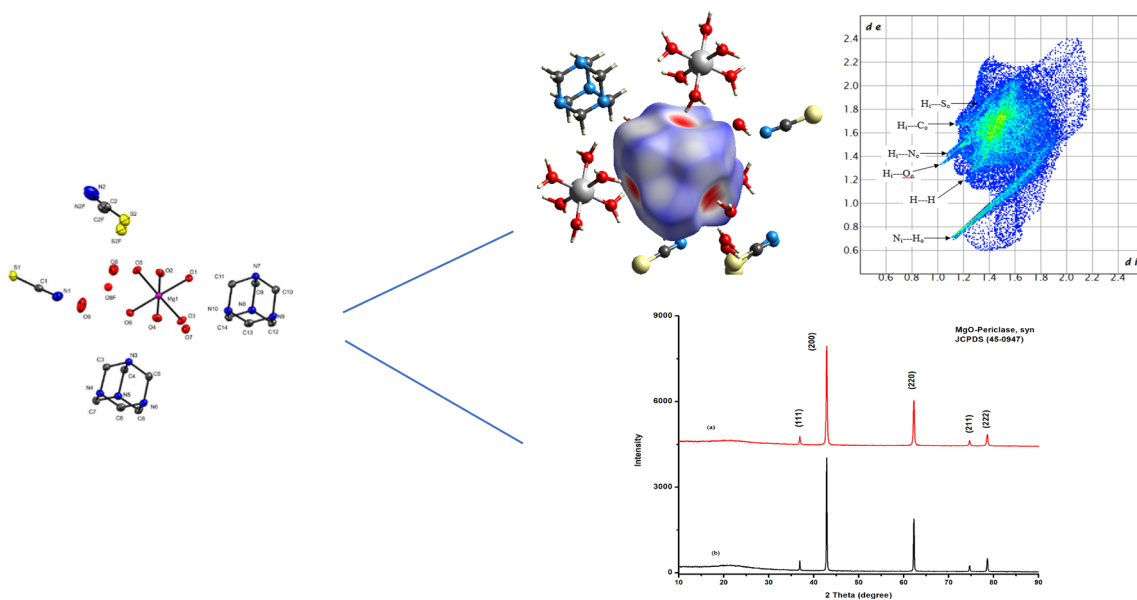
✉ Divine Mbom Yufanyi
  dyufanyi@yahoo.com

Extended author information available on the last page of the article

Introduction

The coordination chemistry of the s-block metals recently experienced intense research focus, due to their properties and potential applications in diverse domains such as medicine, catalysis, organometallic synthesis, nanotechnology, industry, and research.(Fromm 2008; Kruszynski et al. 2012, 2015; Westerhausen 2017); The significant roles played by alkali metal ions such as Li$^+$, Na$^+$, and K$^+$ in different biological processes, have rendered their coordination chemistry to be very important, while that of alkaline earth metals is a result of their application in pigments and pharmaceuticals owing to their lower toxicity, lower cost, etc., over the transition and lanthanoid metals.(Fromm 2008; Kruszynski et al. 2015; Shah et al. 2019).

The idea that alkali and alkaline earth metals form stable complexes predominantly with O-donor ligands as compared to N-donor ligands slowed the development of this chemistry. There is a recent surge in the chemistry of these metals, especially towards N-donor ligands, since heterocyclic N-donor ligands can be used as model ligands for many bioactive processes.(Das et al. 2013) An expansion of

this research domain is important to understand the types of interactions and structure types formed by these metal ions with bioactive molecules. Likewise, information acquired on the coordination chemistry of these metal ions, with other ligands, will permit us to make comparisons of their coordination patterns and properties to those of transition metals, since s-block metal–organic compounds already find applications in pigments and pharmaceuticals.(Fromm 2008) Also, this will enable the acquisition of relevant information on the useful properties of dinuclear, multinuclear, and polymeric coordination compounds of s-block metals.(Czubacka et al. 2011; Ezzayani et al. 2021; Mengle et al. 2014; Read et al. 2014; Underwood et al. 2014) The interaction of these metals with neutral ligands as well as an understanding of the factors that drive self-organization in the supramolecular structures formed, is of interest, given the importance of these metals in medicine and nanotechnology.(Ezzayani et al. 2021; Leonarski et al. 2019; Rodzik et al. 2020).

Different ligands have been employed in the construction of supramolecular networks with s-block elements. Amongst these ligands used, hexamethylenetetramine (HMTA), a cost-effective, benign, and readily available heterocyclic
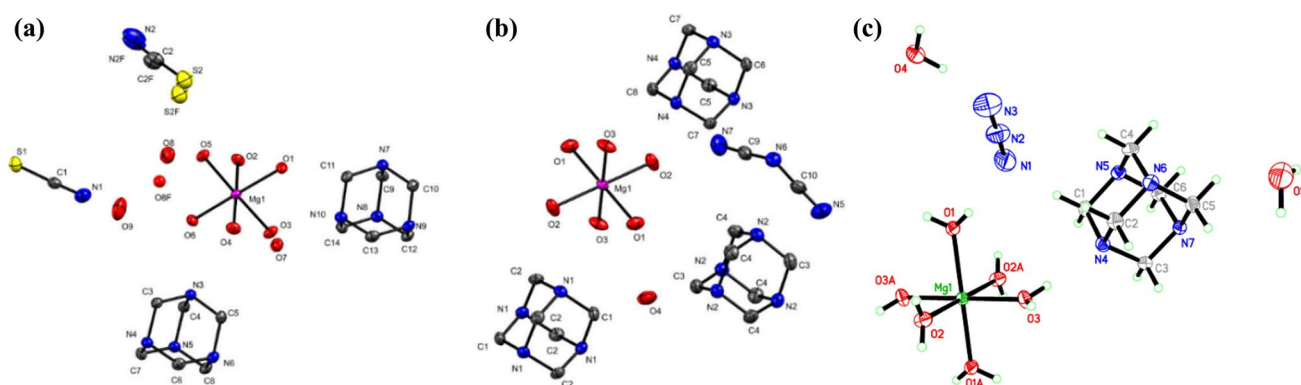

Fig. 1 ORTEP diagrams of (**a**) **1a** (**b**) **1b** and (**c**) **1c** with the atom-numbering schemes. The thermal ellipsoids are drawn at the 50% probability level
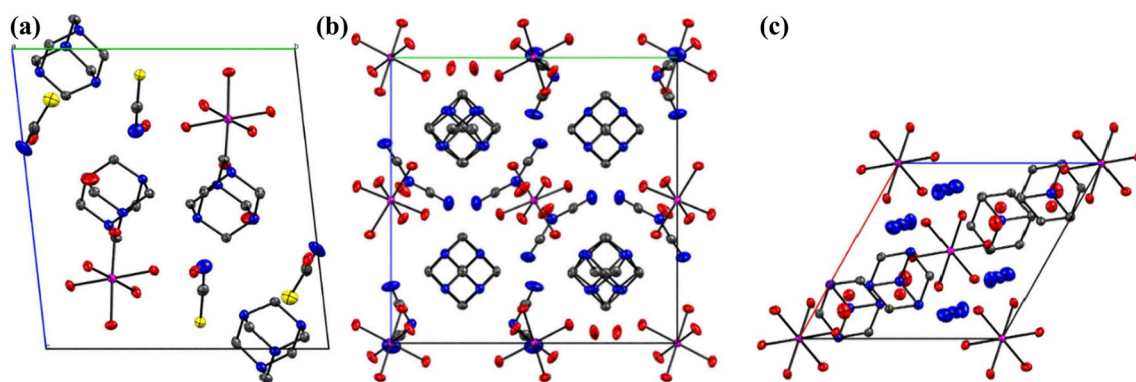

Fig. 2 Packing diagrams of (**a**) **1a** (**b**) **1b** and (**c**) **1c**

Table 1 Crystal data, data collection, and structure refinement details

1a		1b	1c
Chemical formula	$C_{14}H_{42}MgN_{10}O_9S_2$	$C_{16}H_{40}MgN_{14}O_8$	$C_{12}H_{44}MgN_{14}O_{10}$
Molecular weight (M_r)	583.00	580.93	568.92
Crystal system, space group	Triclinic, $P1$	Tetragonal, $P4_2/n$	Monoclinic, $P2_1/n$
Temperature (K)	130	130	150(2) K
a, b, c (Å)	9.3678 (4), 12.0438 (4), 12.9104 (5)	14.1307 (2), 14.1021 (4)	9.1901(3), 18.8179(6), 9.2638(3)
α, β, γ (°)	81.865 (3), 79.364 (3), 80.004 (3)	90	119.5188(11)
V (Å^3)	1400.80 (10)	2815.86 (11)	1394.11(8)
Z	2	4	2
Radiation type	Mo $K\alpha$	Mo $K\alpha$	Mo $K\alpha$
μ (mm^{-1})	0.27	0.13	0.133
Crystal size (mm)	$0.30 \times 0.30 \times 0.10$	$0.20 \times 0.20 \times 0.10$	$0.380 \times 0.335 \times 0.275$
Diffractometer	Xcalibur, Sapphire3, Gemini	Xcalibur, Sapphire3, Gemini	Bruker APEX-II CCD
T_{min}, T_{max}	0.992, 1.000	0.989, 1.000	0.990, 1.000
No. of measured, independent and observed [$I > 2\sigma(I)$] reflections	23,677, 9247, 6877	18,893, 4787, 3144	11,474, 2626, 2423
R_{int}	0.027	0.051	0.023
$(\sin \theta/\lambda)_{max}$ (Å^{-1})	0.756	0.759	0.610
$R[F^2 > 2\sigma(F^2)]$, $wR(F^2)$, S	0.060, 0.184, 1.02	0.056, 0.129, 1.04	0.052, 0.152, 1.05
No. of reflections	9247	4787	2626
No. of parameters	499	261	209
H-atom treatment	H atoms treated by a mixture of independent and constrained refinement	All H-atom parameters refined	H atoms treated by a mixture of independent and constrained refinement
$\Delta\rho_{max}$, $\Delta\rho_{min}$ (e Å^{-3})	1.44, -1.27	0.41, -0.41	1.57, -0.41

organic compound with a cage-like structure has been much explored. It has four bridge-head nitrogen atoms with coordination patterns ranging from terminal monodentate to bridging mode between two metal atoms, It is highly soluble in water and polar organic solvents (Kirillov 2011; Yufanyi et al. 2015). HMTA is an excellent hydrogen acceptor with several reports of H-bonded molecular adducts with organic molecules.(Lemmerer 2011; Rivera et al. 2019) While H-bonded networks of transition(Banerjee et al. 2007; Chen et al. 2005; Chopra et al. 2004; Dagur et al. 2003; Ganesh et al. 1990; Hu et al. 2002; Kaihua & Shuhong 2018; Li et al. 2008; Yao et al. 2008; Zhu et al. 2003a, b; Zhu et al. 2003a, b) and lanthanoid (Kumar et al. 2012; Trzesowska-Kruszynska et al. 2010) metals with HMTA have been explored, that of s-block metals is still developing.(Dahan 1974, 1975; Katsaros 1983; Kruszynski et al. 2012, 2015; Sieranski & Kruszynski 2011).

Research interest into understanding the role played and the effects of non-covalent interactions, such as hydrogen bonding (e.g., N–H⋯O, O–H⋯O, and O–H⋯N), weak interactions (e.g. C–H⋯O, C–H⋯N, C–H⋯π, and π⋯π), dipole–dipole, hydrophobic interactions, etc., on the self-assembly of molecular building blocks to generate supramolecular structures, is increasing.(Aakeröy et al. 2010;

Desiraju 1994; Jagan et al. 2021; Janiak and Scharmann 2003; Lu et al. 2010; Whitesides and Boncheva 2002) These interactions have enabled the development of supramolecular networks with diverse structures and functional applications, based on a careful choice of metal ion, ligand, co-ligand, and solvent, which are crucial to the structure types obtained and the interactions therein.

We have been interested in the coordination chemistry of transition metals with N-donor ligands, particularly HMTA. This interest is motivated by the fact that some metal complexes of HMTA had previously been used as precursors for metal dispersions,(Afanasiev et al. 2008) metal carbides and nitrides,(Chouzier et al. 2011) and oxide nanoparticles. (Yufanyi et al. 2014) While interactions between magnesium and HMTA are known,(Kaihua and Shuhong 2018; Katsaros 1983; Sieranski and Kruszynski 2011) the influence of other co-ligands on the non-covalent interactions as well as the structure type, and hence crystal packing has not been explored. Herein, we have made use of reactants with different numbers of atoms (potential acceptors or donors) to produce co-crystallized adducts with diverse non-covalent interactions in the structures, on account of the presence of $Mg(H_2O)_6^{2+}$, H_2O, SCN^- (or N_3^-, or $C_2N_3^-$) and HMTA. Hirschfeld surface analysis was also performed to visualize

Table 2 Selected Bond lengths [Å] and angles [°] for **1a-c**

1a		1b		1c	
Mg(1)–O(6)	2.0402(16)	Mg(1)–O(3)#1	2.0375(13)	Mg(1)-O(3)	2.0400(14)
Mg(1)–O(3)	2.0416(15)	Mg(1)–O(3)	2.0376(13)	Mg(1)–O(3)#1	2.0400(14)
Mg(1)–O(5)	2.0448(15)	Mg(1)–O(1)#1	2.0400(13)	Mg(1)–O(1)	2.0654(14)
Mg(1)–O(4)	2.0559(16)	Mg(1)–O(1)	2.0400(13)	Mg(1)–O(1)#1	2.0654(14)
Mg(1)–O(1)	2.0656(16)	Mg(1)–O(2)#1	2.0623(13)	Mg(1)–O(2)	2.0673(15)
Mg(1)–O(2)	2.0696(16)	Mg(1)–O(2)	2.0623(13)	Mg(1)–O(2)#1	2.0673(15)
O(6)–Mg(1)–O(3)	88.60(7)	O(3)#1–Mg(1)–O(3)	180.0	O(3)–Mg(1)–O(3)#1	180.00(7)
O(6)–Mg(1)–O(5)	93.15(7)	O(3)#1–Mg(1)–O(1)#1	90.50(6)	O(3)–Mg(1)–O(1)	91.30(6)
O(3)–Mg(1)–O(5)	178.24(7)	O(3)–Mg(1)–O(1)#1	89.50(6)	O(3)#1–Mg(1)–O(1)	88.70(6)
O(6)–Mg(1)–O(4)	92.22(7)	O(3)#1–Mg(1)–O(1)	89.50(6)	O(3)–Mg(1)–O(1)#1	88.70(6)
O(3)–Mg(1)–O(4)	88.67(7)	O(3)–Mg(1)–O(1)	90.50(6)	O(3)#1–Mg(1)–O(1)#1	91.30(6)
O(5)–Mg(1)–O(4)	91.06(6)	O(1)#1–Mg(1)–O(1)	180.0	O(1)–Mg(1)–O(1)#1	180.0
O(6)–Mg(1)–O(1)	177.54(7)	O(3)#1–Mg(1)–O(2)#1	89.02(6)	O(3)–Mg(1)–O(2)	91.97(6)
O(3)–Mg(1)–O(1)	89.64(7)	O(3)–Mg(1)–O(2)#1	90.98(6)	O(3)#1–Mg(1)–O(2)	88.03(6)
O(5)–Mg(1)–O(1)	88.62(6)	O(1)#1–Mg(1)–O(2)#1	90.48(6)	O(1)–Mg(1)–O(2)	91.70(6)
O(4)–Mg(1)–O(1)	89.46(7)	O(1)–Mg(1)–O(2)#1	89.52(6)	O(1)#1–Mg(1)–O(2)	88.30(6)
O(6)–Mg(1)–O(2)	87.20(7)	O(3)#1–Mg(1)–O(2)	90.98(6)	O(3)–Mg(1)–O(2)#1	88.03(6)
O(3)–Mg(1)–O(2)	92.01(7)	O(3)–Mg(1)–O(2)	89.02(6)	O(3)#1–Mg(1)–O(2)#1	91.97(6)
O(5)–Mg(1)–O(2)	88.29(6)	O(1)#1–Mg(1)–O(2)	89.52(6)	O(1)–Mg(1)–O(2)#1	88.30(6)
O(4)–Mg(1)–O(2)	179.10(7)	O(1)–Mg(1)–O(2)	90.48(6)	O(1)#1–Mg(1)–O(2)#1	91.70(6)

Symmetry transformations used to generate equivalent atoms: **1b**: #1 -x + 1,-y + 1,-z + 1, **1c**: #1 -x + 2,-y,-z + 2

Supramolecular Features

the short contacts in the supramolecular structures and to determine the relative contributions of the various non-covalent interactions present in the crystal structures using two-dimensional fingerprint plots. The thermal decomposition study of these compounds has also been presented.

Results and discussion

The reaction of the magnesium salt with HMTA and the co-ligand in methanol, at room temperature, afforded the mononuclear compounds **1a–c**, which were found to be air-stable. The compounds were characterized by single-crystal X-ray diffraction, elemental analysis, IR spectroscopy, and thermal analysis. The residues from the thermal analysis were analysed by powder X-ray diffraction.

The molecular structures, along with the atom numbering schemes of **1a–c** are presented in Fig. 1 and the packing diagrams in Fig. 2. While the crystal data are presented in Table 1, selected interatomic distances and angles are listed in Table 2. X-ray crystal structure analysis reveals that **1a–c** crystallize in the triclinic $P1$, tetragonal $P4_2/n$, and monoclinic, $P2_1/n$ space groups, respectively. The structures consist of a complex cation $Mg(H_2O)_6^{2+}$ in addition to two SCN^-, three lattice water molecules and two HMTA molecules for **1a**, two DCA, one lattice water, and three HMTA

molecules for **1b** as well as azide, lattice water, and HMTA molecules for **1c**, assembled into a 3D supramolecular framework through intermolecular H-bonds. The magnesium (II) ion is in a slightly distorted octahedral coordination environment in which both the equatorial plane and trans-axial planes are occupied by four and two coordinated water molecules, respectively.

In the complex cation $Mg(H_2O)_6^{2+}$, the Mg-O bonds [2.0375–2.0696 Å] are within the expected ranges and comparable to literature values.(Sieranski and Kruszynski 2011) The cis-bond angles [87.20(7)–93.15(7)°] around the Mg centers in $Mg(H_2O)_6^{2+}$ for **1a-c** deviate from ideal values, indicating that the octahedra are slightly distorted.

In the crystal structures, several non-covalent interactions exist. Hydrogen bonds abound in the crystal structures of **1a-c** which link the molecules into a 3D supramolecular structure. In **1a** the O–H···N$_{SCN}$, O–H···O and O–H···N$_{HMTA}$ H-bonds are found. Each cation, $Mg(H_2O)_6^{2+}$, is linked through O–H···N$_{SCN}$, O–H···O and O–H···N$_{HMTA}$ H-bonds (Fig. 3, Table 3) to two HMTA, four SCN^- and two water molecules. In addition, C11–H11···S1 H-bonds between HMTA and SCN^- are present. This highly intricate H-bonding network between the cation, water, SCN^-, and HMTA molecules results in chains and rings of different sizes.

The crystal structures of **1b** and **1c** are stabilized by a variety of O–H···N intermolecular H-bonds. The O1 and O3

Fig. 3 Hydrogen bond patterns
in the crystal structure of **1a**
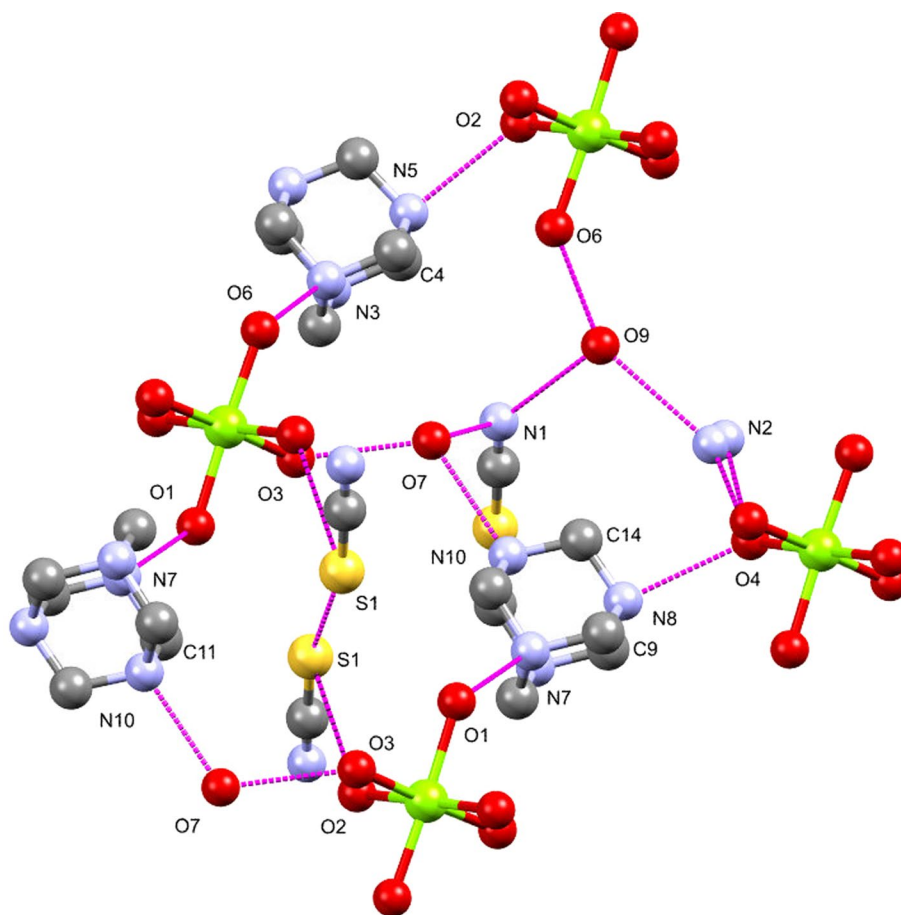
atoms of $Mg(H_2O)_6^{2+}$ in **1b** and **1c** are each H-bonded to one DCA and one HMTA or an azide and one HMTA molecule, respectively, while the other O-atoms are H-bonded to one HMTA and a water molecule. In addition to these, weak C–H···N intermolecular interactions extend the complexes into 3D structures.

IR spectroscopy

The relevant infrared bands of HMTA, the co-ligands, and the complexes are listed in Table 4 while the FTIR spectra of the complexes are shown in Fig. 4. The broad bands at 3426–3452 cm^{-1} are attributed to ν(OH) of coordinated water, while that at 3160 cm^{-1} is assigned to ν(OH) of lattice water (Afanasiev et al. 2008; Ng et al. 2004). The band at 1230 cm^{-1}, assigned to the ν(CH$_2$) rocking vibration of the free HMTA ligand, is observed at 1238, 1243, and 1240 cm^{-1}, respectively in **1a-c**. Strong prominent peaks at 1000 cm^{-1} and 812 cm^{-1} due to the C–N stretching vibration of HMTA are slightly shifted to 1005 cm^{-1} and 813 cm^{-1}, respectively, in the complexes due to changes in the chemical environment.(Agwara et al. 2008) The sharp peak at 2053 cm^{-1} due to the C≡N vibration of free thiocyanate ion was observed at 2084 cm^{-1} in **1a** while the C–S stretching

vibration of the thiocyanate was observed at 751 cm^{-1} in both the free thiocyanate ion and in **1a**. Furthermore, in **1b**, the bands at 2287, 2229, and 2181 cm^{-1} corresponding to $\nu_s + \nu_{as}$ (C≡N), ν_{as}(C≡N) and ν_s(C≡N) of the dicyanamide were observed at 2254, 2219, and 2162 cm^{-1}, respectively. The very strong band at 2106 cm^{-1} assigned to ν_{as} asymmetric NNN stretch was observed at 2080 cm^{-1} in **1c**.

1a-c contain several different chemical species indicating that there are many possibilities of intermolecular interactions. A good description of these intermolecular interactions is necessary to understand how the crystal is stabilized. The qualitative and quantitative analysis of the intermolecular interactions found in **1a-c** was done using 3D Hirschfeld surface analysis and 2D fingerprint map, respectively. The intermolecular interactions were analysed for HMTA and the $\left[Mg(H_2O)_6\right]^{2+}$ cation in the unit cell to compare the chemical environments in the complexes. The visualization of the Hirschfeld 3D d$_{norm}$ surface and the overall 2D fingerprint of these chemical species are presented in Fig. 5 for HMTA and Fig. 6 for $\left[Mg(H_2O)_6\right]^{2+}$.

The analysis of the HS around HMTA (Fig. 5) indicates that all its nitrogen atoms are involved in strong H-bonding with hydrogen atoms of three $\left[Mg(H_2O)_6\right]^{2+}$ cations and one water molecule. There are also weak hydrogen bonds

Table 3 Hydrogen-bond geometry (Å, º) for **1a-c**

D–H···A	D–H	H···A	D···A	D–H···A
1a				
O1–H1^{O1}b···N7^i	0.76 (2)	2.07 (2)	2.823 (2)	169 (3)
O2–H1^{O2}b···S1^{ii}	0.75 (2)	2.56 (2)	3.303 (16)	172 (3)
O2–H2^{O2}b···N5^{iii}	0.75 (2)	2.12 (2)	2.867 (2)	170 (3)
O3–H1^{O3}b···O7	0.76 (2)	1.96 (2)	2.703 (2)	166 (3)
O3–H2^{O3}b···N9^{iv}	0.76 (2)	2.08 (2)	2.836 (2)	175 (4)
O4–H1^{O4}b···N2F^{b}v	0.77 (2)	2.05 (5)	2.80 (4)	165 (3)
O4–H2^{O4}b···N8^{vi}	0.77 (2)	2.03 (2)	2.798 (2)	171 (3)
O5–H2^{O5}b···O8F^{b}	0.79 (2)	1.86 (2)	2.611 (10)	160 (3)
O5–H1^{O5}b···N6^{vii}	0.80 (2)	2.03 (2)	2.821 (2)	167 (3)
O6–H2^{O6}b···O9	0.79 (2)	1.90 (2)	2.672 (3)	167 (4)
O6–H1^{O6}b···N3	0.80 (2)	2.02 (2)	2.803 (2)	167 (3)
O7–H2^{O7}···N1^{iii}	0.78 (2)	2.12 (2)	2.866 (3)	160 (3)
O7–H1^{O7}···N10	0.79 (2)	2.01 (2)	2.799 (2)	174 (3)
O8a–H1^{O8}a···S2a	0.99	2.20	3.178 (2)	171
O8a–H2^{O8}a···N4^{viii}	0.99	1.83	2.807 (3)	170
O9–H2^{O9}···N1	0.81 (2)	2.05 (2)	2.855 (4)	170 (4)
1b				
O1–H1$O1$···O4	0.95 (3)	1.74 (3)	2.676 (2)	171 (3)
O1–H2$O1$···N3^i	0.84 (3)	2.03 (3)	2.841 (19)	165 (2)
O2–H1$O2$···N4	0.86 (3)	2.05 (3)	2.866 (19)	160 (3)
O2–H2$O2$···N7	0.89 (3)	1.88 (3)	2.761 (2)	168 (3)
O3–H1$O3$···N1	0.92 (3)	1.91 (3)	2.814 (19)	169 (3)
O3–H2$O3$···N5^{ii}	0.77 (3)	2.00 (3)	2.760 (3)	172 (3)
O4–H1$O4$···N2	0.89 (4)	2.02 (4)	2.833 (2)	153 (3)
O4–H2$O4$···N6^{iii}	0.81 (4)	2.07 (4)	2.864 (2)	169 (3)
1c				
O5–H10···N2^i	0.92 (4)	2.60 (4)	3.426 (3)	150 (3)
O5–H10···N1^i	0.92 (4)	1.95 (4)	2.872 (4)	176 (4)
O5–H9···N3^{ii}	1.01 (3)	1.79 (3)	2.793 (3)	172 (2)
O5–H9···N2^{ii}	1.01 (3)	2.65 (3)	3.629 (3)	164.3 (19)
O4–H8···N6^{iii}	0.87 (4)	1.96 (4)	2.815 (2)	171 (3)
O3–H6···O4^{iv}	0.90 (3)	1.81 (3)	2.689 (2)	166 (3)
O1–H2···N7^v	0.81 (3)	2.00 (3)	2.797 (2)	167 (3)
O1–H1···N1	0.82 (3)	2.05 (3)	2.849 (3)	168 (3)
O2–H3···N3^{vi}	0.79 (4)	2.11 (4)	2.865 (3)	159 (3)
O2–H4···N5^{vii}	0.80 (5)	2.03 (5)	2.818 (2)	168 (4)
O4–H7···O5^{iii}	0.87 (4)	1.91 (4)	2.777 (3)	173 (3)
O3–H5···N4	0.79 (4)	2.04 (4)	2.815 (2)	168 (3)

Symmetry codes: (i) $-x, -y+1, -z+2$; (ii) $-x, -y+1, -z+1$; (iii) $-x+1, -y+1, -z+1$; (iv) $-x+1, -y+1, -z+2$; (v) $x+1, y, z$; (vi) $x, y-1, z$; (vii) $x-1, y, z$; (viii) $-x+1, -y, -z+1$ for **1a**; Symmetry codes: (i) $-y+3/2, x, -z+3/2$; (ii) $y, -x+3/2, -z+3/2$; (iii) $y+1/2, -x+1, z-1/2$ for **1b**; Symmetry codes: (i) $x+1/2, -y+1/2, z-1/2$; (ii) $x, y, z-1$; (iii) $x-1/2, -y+1/2, z+1/2$; (iv) $x+1, y, z$; (v) $x, y, z+1$; (vi) $x+1/2, -y+1/2, z+1/2$; (vii) $x+1, y, z+1$ for **1c**

involving hydrogen atoms of HMTA, one SCN⁻ and one H₂O for **1a** as well as two N₃⁻ and one H₂O for **1c**. H–H contacts are the most predominant interactions due to the

abundance of hydrogen on the molecular surface, followed by N–H and S–H interactions (in **1a**). Here, the contribution of C–H–X (X=N, O, S) is about 5%. The contribution of these interactions to the Hirshfeld surface is not the same for the HMTA of the asymmetric unit. These results show that, in the crystal packing of **1a-c**, HMTA is mostly engaged in H–H interactions with the surrounding molecules.

The analysis of the 3D Hirschfeld surface around the $\left[Mg(H_2O)_6\right]^{2+}$ cation of **1a-c** reveals the presence of an intense red spot around each hydrogen atom of the complex ion. Hence, all these hydrogen atoms are involved in strong hydrogen bonds with neighbouring chemical species. For **1b** and **1c**, six of these hydrogen bonds are formed with nitrogen atoms of six HMTA, four with nitrogen atoms of four anions and the other two with the oxygen atoms of two water molecules. In **1a**, the same atoms are involved except that there are 3 water molecules and 3 SCN⁻ (one interacts with N atom and 2 with S atom). The white areas of the HS of **1a-c** indicate the presence of H–H interactions. These interactions are identified on the 2D fingerprint of these molecules by the tips at $d_i + d_e$ between 2.4 and 2.7 Å which is higher or equal to twice the van der Waals radius of hydrogen atom. Thus, the H–H interactions present in **1a-c** are attractive van der Waals interactions. Therefore, they participate in the molecular self-assembly process and contribute to the stabilization of the crystal packing.

The contributions of these different interactions obtained from the decomposition of the 2D fingerprints are presented in Table 5. The H–H intermolecular interactions are the most prevalent in these crystal structures followed by N–HOH interactions. However, for **1b** all the hydrogen bonds constitute about 55% of the Hirshfeld surface of the $\left[Mg(H_2O)_6\right]^{2+}$ cation, while it is 45% of the Hirshfeld surfaces of **1a** and **1c**.

To better appreciate the intermolecular interactions responsible for the crystal packing structure, the nature of the contacts was analyzed by considering the Hirshfeld surface around all the molecules and ions of the asymmetric unit as well as the 2D fingerprint. The results are presented in Fig. 7. The percentage contribution of the contacts to the HS obtained from the decomposition of the 2D fingerprint of **1a**, **1b** and **1c** are summarized in Table 5. From the HS, we observe that strong hydrogen bonds, weak hydrogen bonds, and H–H contacts are all present in the crystal packing of these compounds. H–H interactions are most prevalent, followed by N–H and S–H (**1a**) interactions. In the crystal packing of **1a**, all hydrogen bonds are slightly predominant (4.4 percent) compared to H–H contacts, while in **1b** and **1c** H–H and all hydrogen bonds have almost the same contribution. The difference between the contributions of hydrogen bonds and H–H contacts is 0.5% and 2.6% for **1b** and **1c** respectively. C–H–X (N, O, S) weak interactions contribute less (‹10%) to the crystal packing of **1a** and **1b** and it is absent in **1c**.

Table 4 Selected IR Bands for the Ligands and the Compounds

HMTA	SCN	DCA	N$_3$	1a	1b	1c	Band assignment
–	–	–	–	3426 3160	3452 3284	-3025	υ_s(O–H) (coordinated water) ν(OH) (lattice water)
–	3032	–	–	–	–	–	N–H symmetric stretching
2951	–	–	–	2957	2961	–	ν(CH$_2$)
2873	–	–	–	2886	2888	–	ν(CH$_2$)
–	–	2287	–	–	2254	–	$\nu_s + \nu_{as}$ (CN)
–	–	2229	–	–	2219	–	ν_{as} (CN)
–	–	2181	–	–	2162	–	ν_s (CN)
–	–	–	2106	–	–	2080	ν_{as} asymmetric NNN stretch
–	–	–	1474	–	–	1689	ν_{as} symmetric NNN stretch
–	2050			2095	–	–	SCN Stretching
–	–	–	–	1671	1692	–	HOH bend (lattice water)
1455	–	–	–	1463	1465	1469	ν(CH$_2$) scissor (HMTA)
1369	–	–	–	1380	1376	1375	ν(CH$_2$) wag (HMTA)
1230	–	–	–	1234	1240	1235	ν(CH$_2$) rock (HMTA)
1000	–	–	–	1010	1008	1007	ν(CN) stretch (HMTA)
812	–	–	–	814	813	–	ν(CN) stretch (HMTA)
–	751	–	–	751	–	–	C–S of SCN
–	–	–	–	683	683	693	υ(M–O)

Hirshfeld Surface Analysis
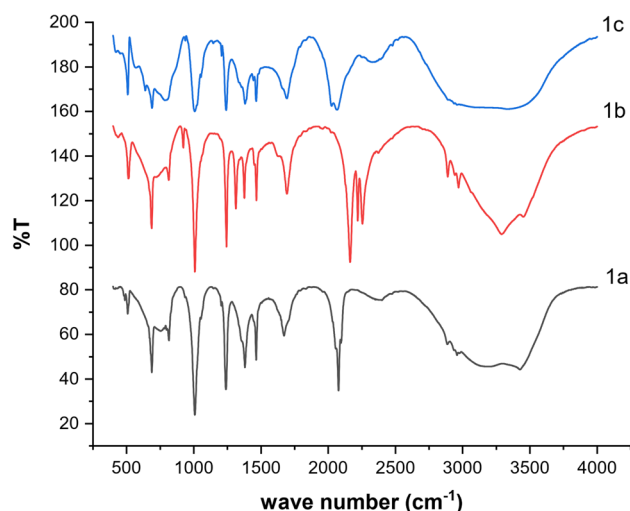
Fig. 4 IR spectra of the complexes

Thermogravimetric analysis

The thermoanalytical curves TG–DTA of **1a-b** are presented in Fig. 8 and the data are summarized in Table 6. Both samples decompose in several steps. These thermograms are characterized by endothermic peaks between 130 and 170 °C for **1a** and at 170 °C for **1b**. The exothermic processes that follow reveal huge mass losses. The endothermic processes that occur within the temperature range 100–190 °C are attributed to the successive loss of both lattice and coordinated water molecules.

The next decomposition step, for **1a**, in the range 200–280 °C with mass loss of 26.33% corresponds to the loss of HMTA molecule (Calc. 26.51). The mass loss of 16.07% between 280 and 340 °C is probably due to the loss of two H$_2$O and CO$_2$ molecules (Calc. 15.15%). In the temperature range 380-740 °C which, from the derivative TG plots, consists of several overlapping decomposition steps, there is a mass loss of 32.55% which can be assigned to the decomposition of carbon material and thiocyanate molecule (Calc. 34.02%) in the form of a mixture of gases (CO$_2$, CO, SO$_2$). A 7.04% residue (Calc. 6.80%) is left.

The TG and DTA curves of **1b** show the removal of 6 water molecules corresponding to a mass loss of 19.08% in the temperature region 130–180 °C (Calc. 18.62%). The mass loss of 24.46% in the region 200–280 °C can be attributed to the decomposition of HMTA marked by a broad exotherm. Another mass loss of 21.76% is observed at about 300–430 °C which is assigned to the loss of three CO$_2$ molecules (Calc. 22.75%). A final mass loss of 27.79% at 450–750 °C can be assigned to the loss of 2 NO$_2$, CO$_2$, and CO (Calc. 28.27%) with a 7% solid residue (Calc. 7.4%).

Powder XRD

The PXRD patterns of the residues (Fig. 9) indicate that they are highly crystalline with well-defined diffraction patterns, and the peaks could be indexed to the MgO cubic
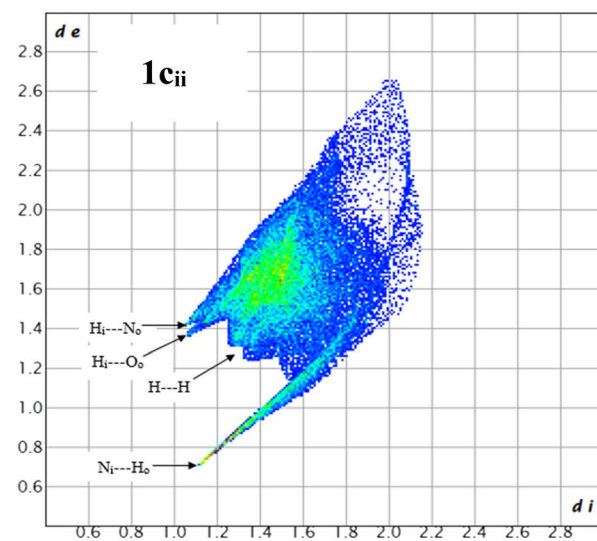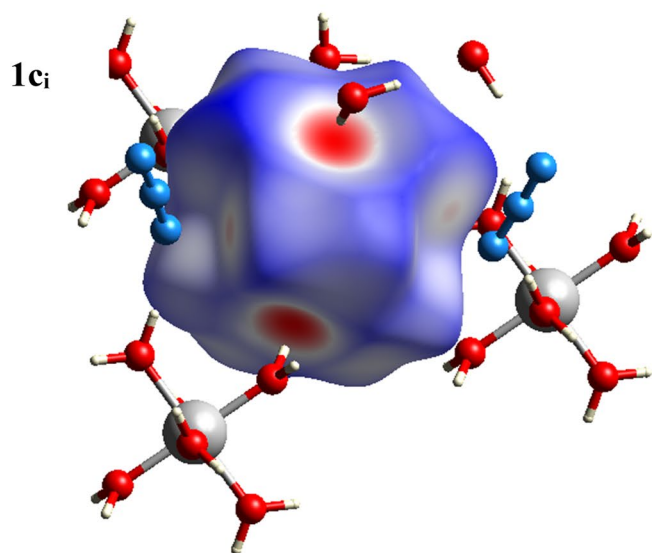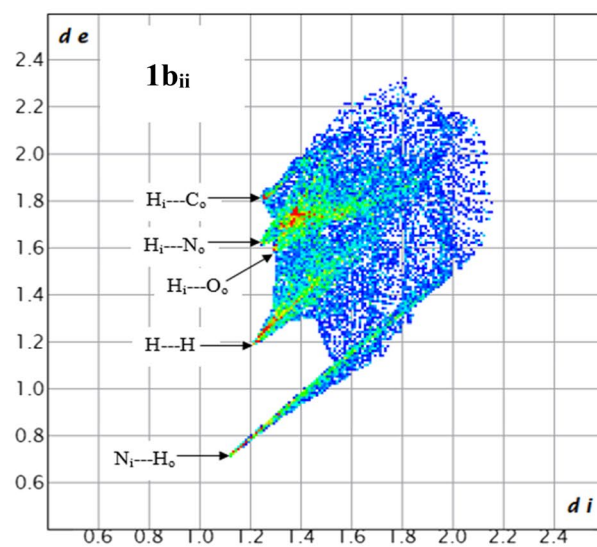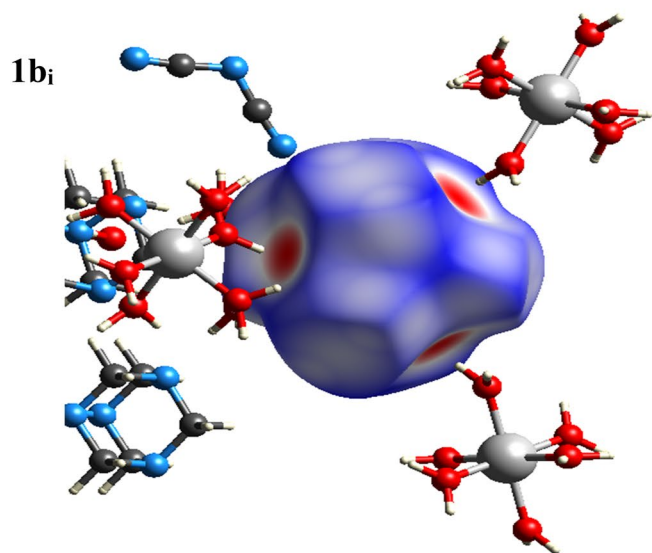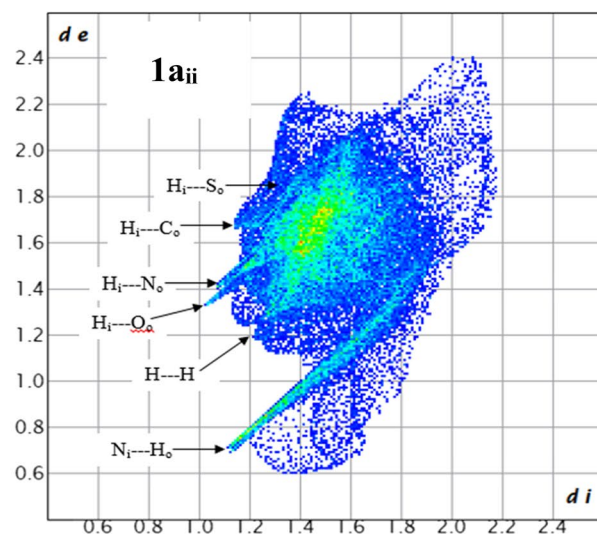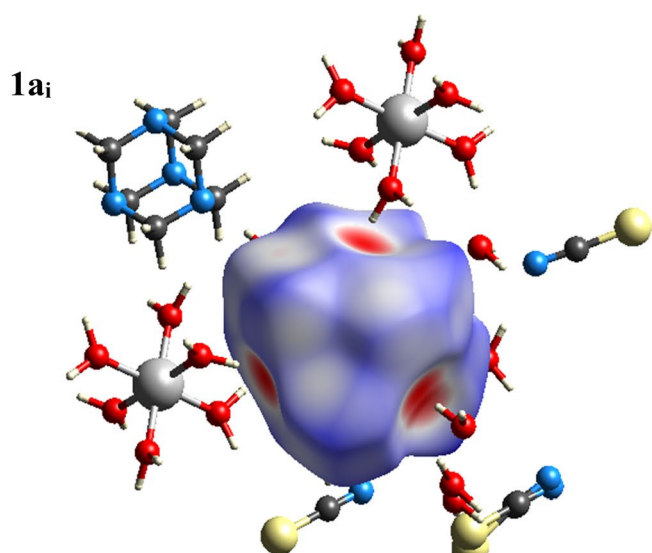
◄**Fig. 5** Hirschfeld surface around HMTA for **1a-c** (1) and their overall 2D fingerprint plot (2) (i = atom is inside the HS; o = the atom is outside the HS; arrows indicate the shortest distance ($d_e + d_i$) between two types of atoms in contacts.)

phase. The peaks for MgO at 36.94, 42.90, 62.30, 74.67, and 78.61correspond to the (111), (200), (220), (211), and (222) crystals planes and match the JCPDS (45–0947).(Khandolkar et al. 2015) The average crystallite sizes of 28.5 nm and 44.8 nm, respectively, for **1a** and **1b**, were calculated from the peak-width at half-height of the (200) peaks, using the Debye–Scherrer equation.

Conclusions

The hydrated magnesium compounds **1a–c**, with $\left[\text{Mg}(\text{H}_2\text{O})_6\right]^{2+}$ as cation, have been synthesized in which all the HMTA ligands are in the outer coordination sphere, H-bonded to water molecules and the co-ligands SCN^-, DCA^- or N_3^-, also present in the outer coordination sphere. The presence and number of the different co-ligands in the complexes affect the number and types of intermolecular interactions present in the crystal structures. Hirshfeld surface analysis indicates that H–H intermolecular interactions are the most prevalent in these crystal structures followed by N–HOH interactions. These hydrogen bonds constitute about 55% of the Hirshfeld surface of the $\left[\text{Mg}(\text{H}_2\text{O})_6\right]^{2+}$ cation for **1b**, while it is 45% of the Hirshfeld surfaces of **1a** and **1c**. The Hirshfeld surface around HMTA indicates that all its nitrogen atoms are involved in strong H-bonding with hydrogen atoms of three $\left[\text{Mg}(\text{H}_2\text{O})_6\right]^{2+}$ cations and one water molecule. There are also weak hydrogen bonds involving hydrogen atoms of HMTA, one SCN^- and one H_2O for **1a** as well as two N_3^- and one H_2O for **1c**. H–H contacts are the most predominant interactions due to the abundance of hydrogen on the molecular surface, followed by N–H and S–H interactions (in **1a**). **1a** and **1b** decompose in a comparable manner in air and the same decomposition product (MgO nanoparticles) is obtained. This indicates that these compounds can be used as suitable precursors for MgO nanoparticles.

Experimental

Materials

Hexamethylenetetramine (HMTA, $C_6H_{12}N_4$) was obtained from Prolabo while, magnesium (II) nitrate hexahydrate ($Mg(NO_3)_2\cdot6H_2O$), and Ammonium thiocyanate (NH_4SCN), were obtained from Riedel-de Haën, sodium dicyanamide ($NaN(CN)_2$), and sodium azide (NaN_3) were obtained from

Sigma Aldrich. All the chemicals were of reagent grade and were used without further purification. All solvents used were dried and distilled according to standard methods.

Synthesis of [Mg(H$_2$O)$_6$](SCN)$_2$·2HMTA·3H$_2$O (**1a**).
$Mg(NO_3)_2\cdot 6H_2O$ (1 mmol, 0.25 g) in 10 mL of methanol was added dropwise to 10 mL methanol solution of HMTA (2 mmol, 0.2803 g) and stirred for 30 min. NH_4SCN (2 mmol, 0.15 g) in 10 mL methanol was added to the mixture and further stirred for 2 h 30 min. The white precipitate formed was filtered, washed with MeOH, and dried in a desiccator over silica gel. Slow evaporation of the filtrate at room temperature afforded **1a** as colorless crystals (80%), m.p. 209°C: Elemental anal. calcd (%) for $C_{14}H_{42}MgN_{10}O_9S_2$ (583.00): C 31.76, H 6.81, N 26.48; found: C 31.26, H 6.15, N 26.52.

Synthesis of [Mg(H$_2$O)$_6$](DCA)$_2$·3HMTA·H$_2$O (**1b**).
This was synthesized following the same procedure as for **1a** but using $NaN(CN)_2$ (2 mmol, 0.18 g). The white precipitate formed was filtered, washed with MeOH, and dried in a desiccator over silica gel. Slow evaporation of the filtrate at room temperature afforded **1b** as colorless crystals (85.2%): Elemental anal. calcd (%) for $C_{16}H_{40}MgN_{14}O_8$ (580.93): C 33.0, H 6.89, N 33.74; found: C 32.85, H 6.43, N 33.01.

Synthesis of [Mg(H$_2$O)$_6$](N$_3$)$_2$·2HMTA·4H$_2$O (**1c**).
This was synthesized following the same procedure as for **1a** but using NaN_3 (2 mmol, 0.13 g). Slow evaporation of the filtrate at room temperature afforded **1c** as colorless crystals (82.6%): Elemental anal. calcd (%) for $C_{12}H_{44}MgN_{14}O_{10}$ (568.92): C 25.31, H 7.73, N 34.45; found: C 25.04, H 7.37, N 33.92.

Characterization

The melting point temperature was recorded using the Leica VMHB Kofler system. Elemental analysis (C, H, N) was carried out on a Flash 2000 Thermo Scientific analyzer while IR spectra of samples, as KBr pellets prepared in a nitrogen-filled glove box, were recorded on a Perkin–Elmer System 2000 FTIR spectrometer in the range 400–4000 cm^{-1}. Thermogravimetric measurements were obtained using a Pyris 6 PerkinElmer TGA 4000 thermal analyzer. The TGA analysis was conducted between 30 and 900 °C in air at a flow rate of 20 mL/min and a temperature ramp of 10 °C/min. Powder XRD measurements were performed with a Stoe-StadiP powder diffractometer with a CuKα (154.0598 pm) X-ray source (0.5°/step and 30 s/step (2 repetitions); tube power: 40 kV/40 mA; scan mode: Debye–Scherrer) using borosilicate glass capillary as sample holder during the measurement. The powder diffraction patterns were analyzed with the help of the STOE powder diffraction system software in combination with the ICDD powder diffraction database (International Centre for Diffraction Data).
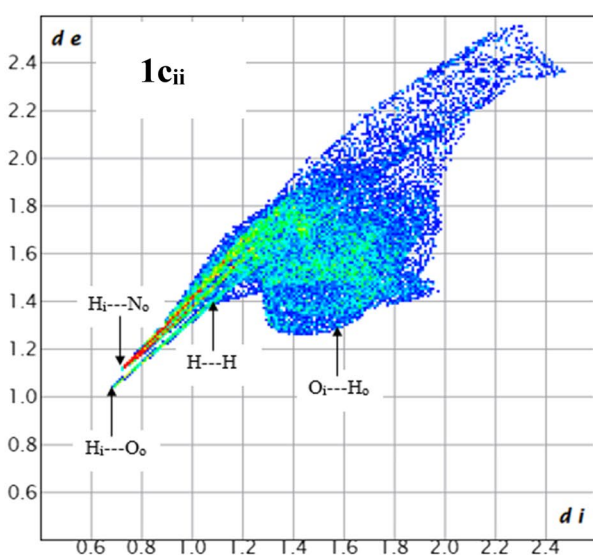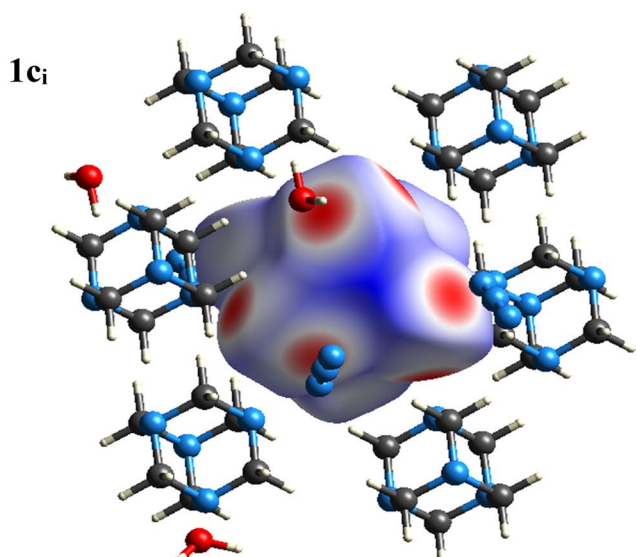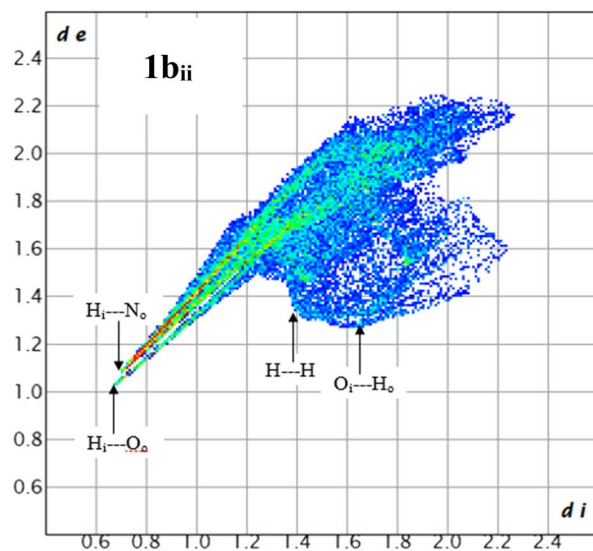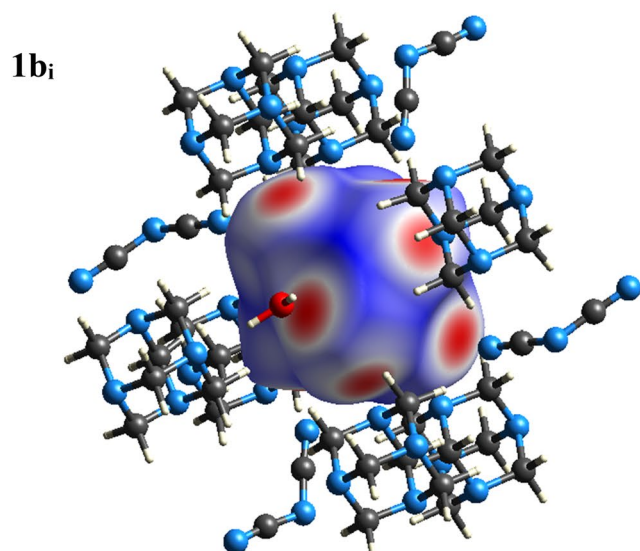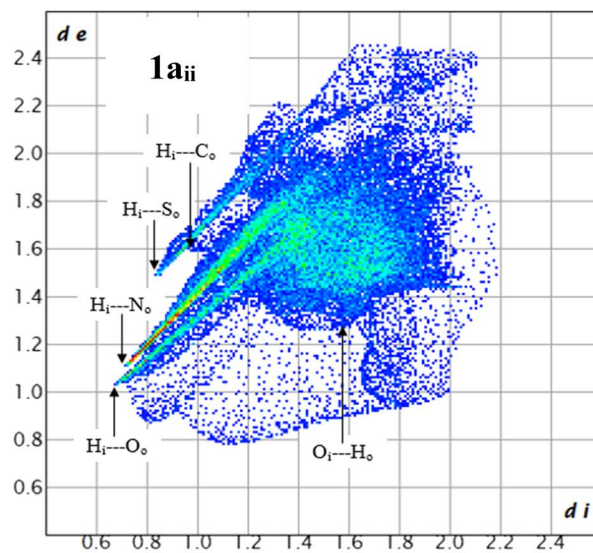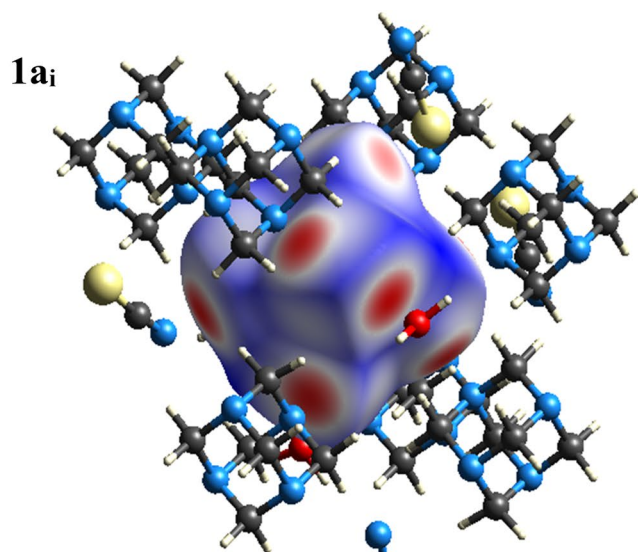
1a_i

1a_ii

1b_i

1b_ii

1c_i

1c_ii

Single crystal X-ray structure

Single Crystal X-ray data were collected with an Xcalibur, Sapphire3, Gemini diffractometer $\lambda(Mo\text{-}K_\alpha) = 0.71073$ Å, $T = 130$ K for **1a** and **1b**, and a GEMINI CCD diffractometer (Rigaku Inc.), $\lambda(Mo\text{-}K\alpha) = 0.71073$ Å, $T = 150(2)$ K, ω-scan rotation for **1c**. Data reduction was performed with CrysAlis Pro including the program SCALE3 ABSPACK for empirical absorption correction. (CrysAlisPro 2013). All structures were solved by dual-space methods with SHELXT-20xy while structure refinement was done with SHELXL-2018 by using full matrix least-square routines against F^2. (Sheldrick 2015) The pictures were generated with the program Mercury (Macrae et al. 2006). **CCDC 2, 159, 208** for **1a**, **2, 159, 209** for **1b**, and **1, 485, 334** for

1c contain the supplementary crystallographic data for this paper. These data can be obtained free of charge via www. ccdc.cam.ac.uk/data_request/cif (or from the Cambridge Crystallographic Data Centre, 12 Union Road, Cambridge CB2 1EZ, UK; fax: (+44)1223-336-033; or deposit@ccdc. cam.uk).

Hirshfeld surface (HS) analysis

A Hirshfeld surface analysis was performed to visualize the different types of interactions present within the structures of **1a–c** using the CrystalExplorer 21.5 software (Spackman et al. 2021) software. Hirshfeld surface(McKinnon et al. 1998; Spackman and Byrom 1997)and the fingerprint plot (McKinnon et al. 2004; Spackman and McKinnon 2002) together constitute a powerful resource for visualizing, exploring, analyzing, and quantifying intermolecular interactions in molecular crystals(McKinnon et al. 2007) and therefore they can be used to compare molecular crystal structures containing similar atoms(Collins et al. 2010; McKinnon et al. 2007; Parkin et al. 2007).

Table 5 Contribution (%) of the different contacts to the Hirshfeld surface around HMTA, $\left[Mg\left(H_2O\right)_6\right]^{2+}$ and all chemical species of the unit cell

		H–H	N–H/N–H	O–H/O–H	C–H/C–H	S–H/S–H
1a	HMTA	63.9	13.9	4.1	5.5	12.7
	$\left[Mg\left(H_2O\right)_6\right]^{2+}$	56.2	20.4	13.5	1.6	8.2
	Unit Cell	46.6	22.5	5.8	7.7	16.2
1b	HMTA	60.8	30.2	6.3	2.7	–
	$\left[Mg\left(H_2O\right)_6\right]^{2+}$	46.1	39.8	14.1	0.0	–
	Unit Cell	50.5	34.7	5.3	8.2	–
1c	HMTA	64.6	26.0	9.4	–	–
	$\left[Mg\left(H_2O\right)_6\right]^{2+}$	55.4	32.8	10.8	–	–
	Unit Cell	52.6	32.9	14.5	–	–
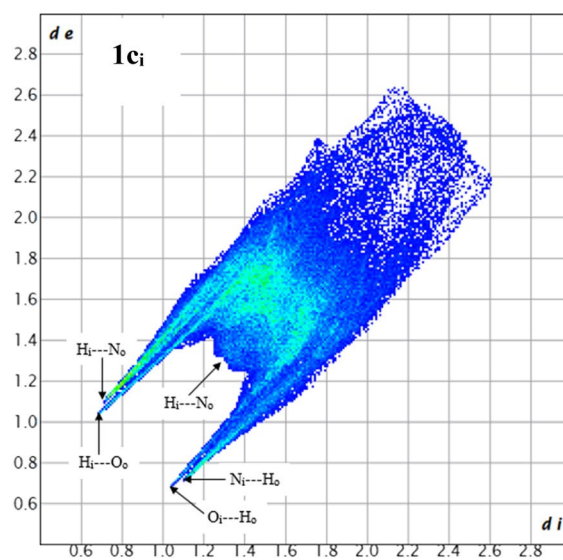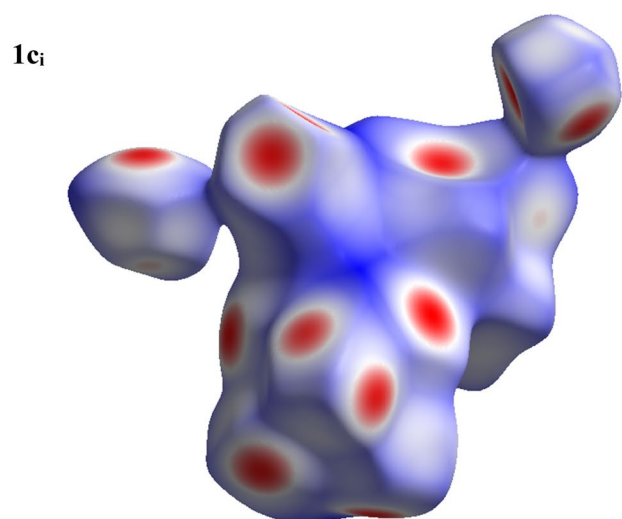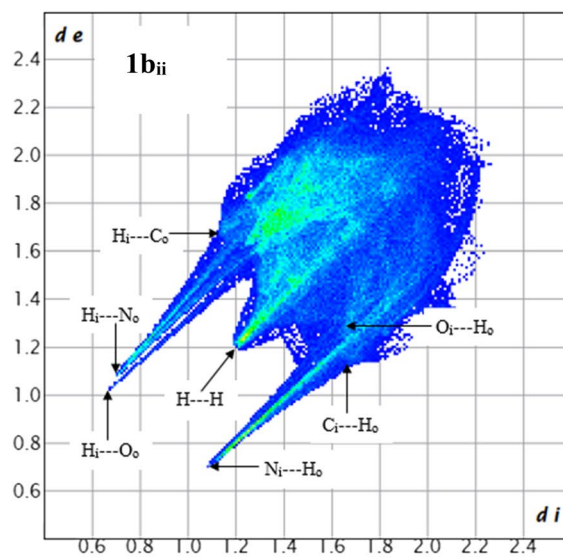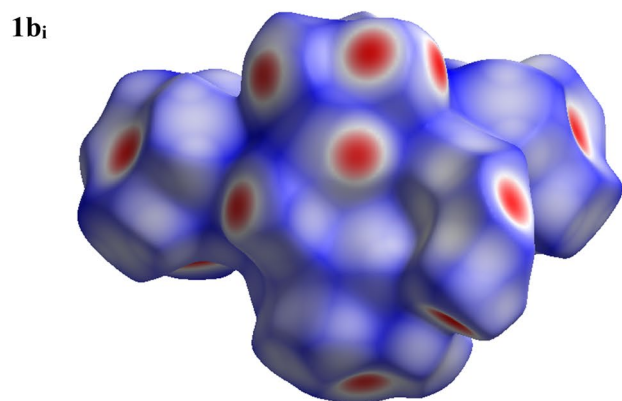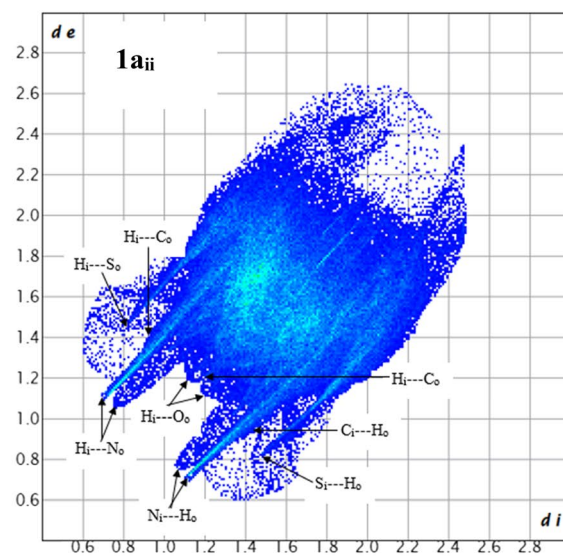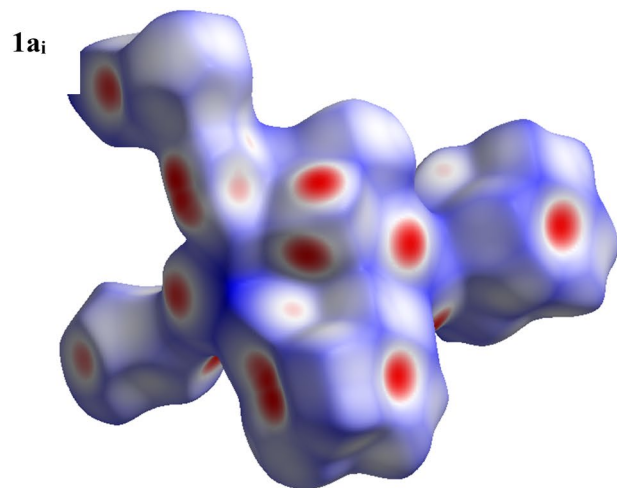
◄**Fig. 7** Hirshfeld surface (1) around all the chemical species of **1a–c** and their (2) 2D fingerprints (i = atom is inside the HS; o = the atom is outside the HS; arrows indicate the shortest distance $(d_e + d_i)$ between two types of atoms in contacts.)

Table 6 Thermal decomposition data for the precursor complexes

Complex	Step	Temperature range (°C)	% Mass Loss	
			Observed	calculated
1a	i	100–180	17.94	18.52
	ii	200–280	26.40	26.51
	iii	280–340	16.07	15.15
	iv	380–740	32.55	34.02
1b	i	130–180	19.08	18.62
	ii	200–290	24.46	24.13
	iii	300–430	21.76	22.75
	iv	450–780	27.79	28.27
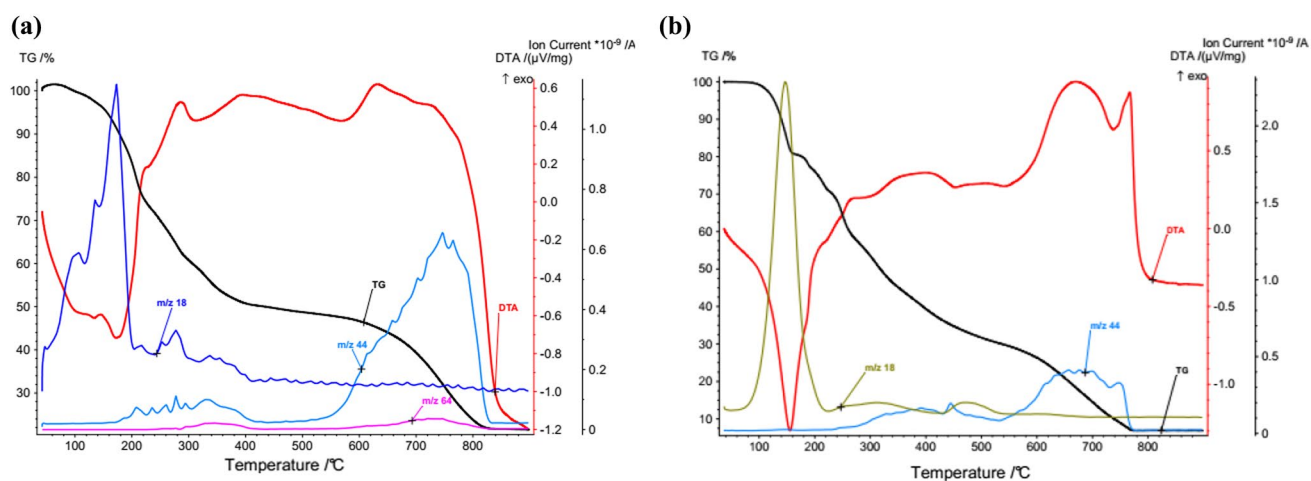
Fig. 8 TGA and DTA curves for **1a** and **1b**

Fig. 9 PXRD patterns of **1a–b**
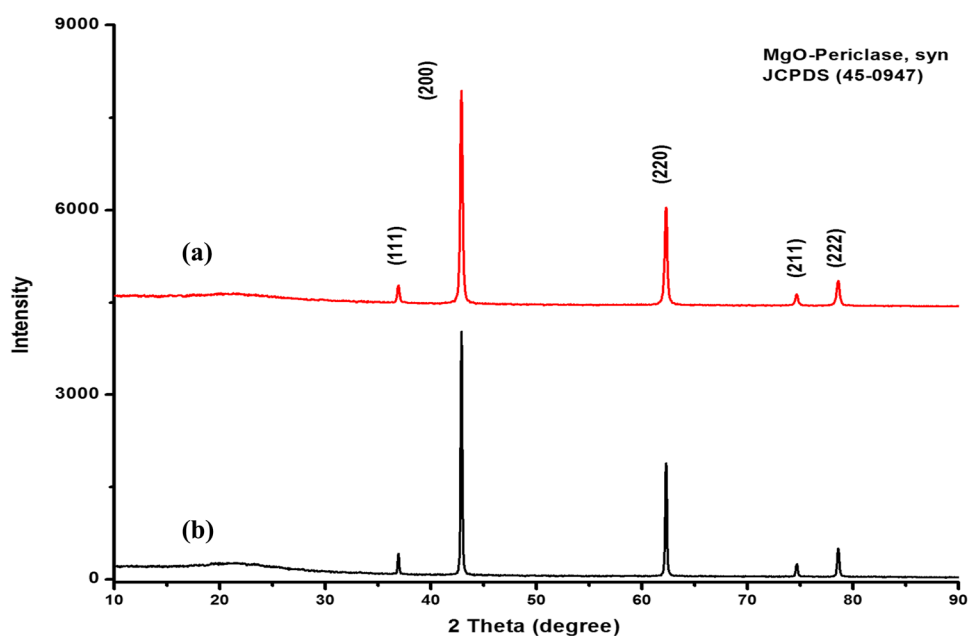
Declarations

Conflict of interests The authors have no competing interests to declare that are relevant to the content of this article.

References

Aakeröy CB, Champness NR, Janiak C (2010) Recent advances in crystal engineering. CrystEngComm 12(1):22–43. https://doi.org/10.1039/b919819a

Afanasiev P, Chouzier S, Czeri T, Pilet G, Pichon C, Roy M, Vrinat M (2008) Nickel and cobalt hexamethylentetramine complexes $(NO_3)_2Me(H_2O)_6(HMTA)_2\cdot 4H_2O$ (Me = Co^{2+}, Ni^{2+}): New Molecular precursors for the preparation of metal dispersions. Inorg Chem 47(7):2303–2311. https://doi.org/10.1021/ic7013013

Agwara MO, Ndifon P, Ndikontar M, Atamba MA (2008) Synthesis, characterisation and antimicrobial activities of Co(II), Ni(II), and Cu(II) complexes of hexamethylenetetramine ligand. Res J Chem Environ 12:87–92

Banerjee S, Choudhury AR, Guru Row TN, Chaudhuri S, Ghosh A (2007) Three-dimensional supramolecular H-bonding network in the compounds containing hexamethylenetetramine and aquated Ni(II) or Cd(II) salts. Polyhedron 26(1):24–32. https://doi.org/10.1016/j.poly.2006.07.019

Chen Z-L, Li S-B, Qiu Z-H, Zeng Q-F, Liang F-P (2005) Hexaaquamanganese(II) dichloride bis(hexamethylenetetramine) tetrahydrate. Acta Crystallog E 61(10):m1931–m1932. https://doi.org/10.1107/s1600536805027571

Chopra D, Dagur P, Prakash AS, Guru Row TN, Hegde MS (2004) Hexaaquamanganese(II) dinitrate bis(hexamethylenetetramine) tetrahydrate. Acta Crystallog E 60(4):m348–m349. https://doi.org/10.1107/s1600536804004337

Chouzier S, Vrinat M, Cseri T, Roy-Auberger M, Afanasiev P (2011) HDS and HDN activity of (Ni, Co)Mo binary and ternary nitrides prepared by decomposition of hexamethylenetetramine complexes. Appl Catal Gen A: 400(1):82–90. https://doi.org/10.1016/j.apcata.2011.04.023

Collins A, Wilson CC, Gilmore CJ (2010) Comparing entire crystal structures using cluster analysis and fingerprint plots. CrystEngComm 12(3):801–809. https://doi.org/10.1039/b914683k

CrysAlisPro (2013) Data collection and processing software package. Rigaku Oxford Difraction

Czubacka E, Kruszynski R, Sieranski T (2011) The structure and thermal behaviour of sodium and potassium multinuclear compounds with hexamethylenetetramine. Struct Chem 23(2):451–459. https://doi.org/10.1007/s11224-011-9888-7

Dagur P, Chopra D, Prakash AS, Guru Row TN, Hegde MS (2003) Hexaaquanickel(II) dichromate bis(hexamethylenetetramine) monohydrate. Acta Crystallog E 59(12):m1129–m1130. https://doi.org/10.1107/s1600536803024875

Dahan F (1974) The crystal structure of the magnesium dichromate hexamethylenetetramine hexahydrate complex. Acta Crystallog. B Struct. Crystallog. Cryst. Chem 30(1):22–27. https://doi.org/10.1107/s0567740874002147

Dahan F (1975) The crystal structure of calcium dichromate bis (hexamethylenetetramine) heptahydrate. Acta Crystallog Sect B: Struct.

Crystallog. Crystal Chem 31(2):423–426. https://doi.org/10.1107/s0567740875002944

Das A, Shit S, Köckerling M, Batsanov AS, Mitra S (2013) Sodium-mediated self-assembly of two nickel(II) schiff base complexes: crystal structure and characterizations. J Coord Chem 66(15):2587–2596. https://doi.org/10.1080/00958972.2013.810731

Desiraju GR (1994) Towards supramolecular inorganic chemistry. Proc Indian Acad Sci 106(3):593–597. https://doi.org/10.1007/bf02911089

Ezzayani K, Ben Khelifa A, Ben Taheur F, Guergueb M, Mansour A, Daran J-C, Nasri H (2021) Building-up novel coordination polymer with magnesium porphyrin: synthesis, molecular structure, photophysical properties and spectroscopic characterization. Potential application as antibacterial agent. Inorg Chim Acta 514:119960. https://doi.org/10.1016/j.ica.2020.119960

Fromm KM (2008) Coordination polymer networks with s-block metal ions. Coord Chem Rev 252(8–9):856–885. https://doi.org/10.1016/j.ccr.2007.10.032

Ganesh V, Seshasayee M, Aravamudan G, Heijdenrijk D, Schenk H (1990) Structure of hexaaquacobalt(II) dichloride bis(hexamethylenetetramine) tetrahydrate. Acta Crystallog C: Crystal Struct Commun 46(6):949–951. https://doi.org/10.1107/s0108270189009832

Hu M-L, Ye M-D, Ng SW (2002) Hexaaquanickel(II) dinitrate bis(hexamethylenetetramine) tetrahydrate. Acta Crystallogr e: Struct Rep 58(9):m486–m487. https://doi.org/10.1107/s1600536802014071

Jagan R, Sathya D, Sivakumar K (2021) Interplay of hydrogen and halogen bonds in supramolecular framework of oxy-acid based 3-chloroanilinium hydrogen sulfate, bis(2,5-dichloroanilinium) sulfate and 2,5-dichloroanilinium perchlorate hydrate salts. Crystallog Rep 66(6):991–999. https://doi.org/10.1134/s106377452106016x

Janiak C, Scharmann TG (2003) Supramolecular C-H···O, C-H···N and C-H···Cl interactions in metal compounds with multi-topic poly (pyrazolyl) borate ligands. Polyhedron 22(8):1123–1133. https://doi.org/10.1016/S0277-5387(03)00098-6

Kaihua J, Shuhong B (2018) Coordination compounds of hexamethylenetetramine with metal salts: a review. Johns Matthey Technol Rev 62(1):89–106. https://doi.org/10.1595/205651317x696621

Katsaros N (1983) The interaction of hexamethylenetetramine with platinum group metals. Transit Met Chem 8(6):345–348. https://doi.org/10.1007/bf00618569

Khandolkar SS, Raghavaiah P, Srinivasan BR (2015) Synthesis, characterization and photochemistry of a new heptamolybdate supported magnesium-aqua coordination complex. J Chem Sci 127(9):1581–1588. https://doi.org/10.1007/s12039-015-0918-7

Kirillov AM (2011) Hexamethylenetetramine: an old new building block for design of coordination polymers. Coord Chem Rev 255(15–16):1603–1622. https://doi.org/10.1016/j.ccr.2011.01.023

Kruszynski R, Sieranski T, Bilinska A, Bernat T, Czubacka E (2012) Alkali metal halogenides coordination compounds with hexamethylenetetramine. Struct Chem 23(5):1643–1656. https://doi.org/10.1007/s11224-012-9961-x

Kruszynski R, Sieranski T, Swiatkowski M, Zielak M, Wojciechowski J, Dzierzawska M, Czubacka E (2015) On the coordination behaviour of the hmta toward alkali metal cations in presence of perchlorate anions. J Chem Crystallog 45(10–12):484–494. https://doi.org/10.1007/s10870-015-0618-7

Kumar D, Kapoor IPS, Singh G, Singh UP, Goel N (2012) Lanthanoid metal nitrates with hydrogen bonded hexamethylenetetramine. J Therm Anal Calorim 114(1):5–18. https://doi.org/10.1007/s10973-012-2826-0

Lemmerer A (2011) Seven hexamethylenetetramine (HMTA) complexes with mono- and dicarboxylic acids: analysis of packing

modes of HMTA complexes in the literature. Acta Crystallog B 67:177–192. https://doi.org/10.1107/S0108768111004964

Leonarski F, D'Ascenzo L, Auffinger P (2019) Nucleobase carbonyl groups are poor Mg$(^{2+})$ inner-sphere binders but excellent monovalent ion binders-a critical PDB survey. RNA 25(2):173–192. https://doi.org/10.1261/rna.068437.118

Li ZL, Yao XJ, Wu W, Xuan YW (2008) Hexaaqua-copper(II) dichloride bis-(hexa-methyl-enetetra-mine) tetra-hydrate. Acta Crystallog E 64(Pt 8):m1024. https://doi.org/10.1107/S1600536808020916

Lu J, Liu H-T, Zhang X-X, Wang D-Q, Niu M-J (2010) Important Roles of weak interactions: syntheses and supramolecular structures of four CoII/NiII-thiocyanato compounds. Z Anorg Allg Chem 636(3–4):641–647. https://doi.org/10.1002/zaac.200900286

Macrae CF, Edgington PR, McCabe P, Pidcock E, Shields GP, Taylor R, Towler M, van de Streek J (2006) Mercury: visualization and analysis of crystal structures. J Appl Crystallog 39(3):453–457. https://doi.org/10.1107/s002188980600731x

McKinnon JJ, Spackman MA, Mitchell AS (2004) Novel tools for visualizing and exploring intermolecular interactions in molecular crystals. Acta Crystallogr Sect B 60(6):627–668. https://doi.org/10.1107/S0108768104020300

McKinnon JJ, Jayatilaka D, Spackman MA (2007) Towards quantitative analysis of intermolecular interactions with hirshfeld surfaces. Chem Commun 37:3814–3816. https://doi.org/10.1039/b704980c

McKinnon JJ, Mitchell AS, Spackman MA (1998) Hirshfeld surfaces: a new tool for visualising and exploring molecular crystals. Chem Eur J 4(11):2136–2141

Mengle KA, Longenecker EJ, Zeller M, Zaleski CM (2014) One-dimensional coordination polymers of 12-metallacrown-4 complexes: {Na2(L)2[12-MCMnIII(N)shi-4]}n, where L is either −O2CCH2CH3 or −O2CCH2CH2CH3. J Chem Crystallog 45(1):36–43. https://doi.org/10.1007/s10870-014-0560-0

Ng CH, Teoh S, Moris N, Yap S (2004) Structural, infrared spectral and thermogravimetric analysis of a hydrogen-bonded assembly of cobalt(II) and nickel(II) mixed complex cations with hexamethylenetetraamine and aqua ligands: {[M(hmt)2(H2O)4][M(H2O)6]}(SO4)2·6H2O. J Coord Chem 57:1037–1046. https://doi.org/10.1080/00958970412331281791

Parkin A, Barr G, Dong W, Gilmore CJ, Jayatilaka D, McKinnon JJ, Spackman MA, Wilson CC (2007) Comparing entire crystal structures: structural genetic fingerprinting. CrystEngComm 9(8):648–652. https://doi.org/10.1039/b704177b

Read CM, Smithzur Loye H-C. MD (2014) Single Crystal growth and structural characterization of a novel mixed-valent ternary uranium oxide, K$_8$U$_7$O$_{24}$. J Chem Crystallog 44(11–12):604–608. https://doi.org/10.1007/s10870-014-0555-x

Rivera A, Rojas JJ, Sadat-Bernal J, Rios-Motta J, Bolte M (2019) Mechanochemical synthesis and X-ray structural characterization of three 3-nitrophenol cocrystals with three aminal cage azaadamantanes: the role of the stereoelectronic effect on intermolecular hydrogen-bonding patterns. Acta Crystallogr C Struct Chem 75(Pt 12):1635–1643. https://doi.org/10.1107/S205322961901516X

Rodzik A, Pomastowski P, Sagandykova GN, Buszewski B (2020) Interactions of whey proteins with metal ions. Int J Mol Sci 21(6):2156. https://doi.org/10.3390/ijms21062156

Shah SR, Shah Z, Ullah N, Hussain J, Al-Harrasi R, Khan A, Rawson JM, Al-Harrasi A, Anwar MU (2019) Crystal structure, shape analysis and bioactivity of new Li(I), Na(I) and Mg(II) complexes with 1,10-phenanthroline and 2-(3,4-dichlorophenyl)acetic acid. Acta Crystallogr c: Struct Chem 75:294–303. https://doi.org/10.1107/S2053229619001396

Sheldrick G (2015) Crystal structure refinement with SHELXL. Acta Crystallogr C 71(1):3–8. https://doi.org/10.1107/S2053229614024218

Sieranski T, Kruszynski R (2011) Magnesium sulphate complexes with hexamethylenetetramine and 1,10-phenanthroline. J Therm Anal Calorim 109(1):141–152. https://doi.org/10.1007/s10973-011-1693-4

Spackman MA, Byrom PG (1997) A novel definition of a molecule in a crystal. Chem Phys Lett 267(3):215–220. https://doi.org/10.1016/S0009-2614(97)00100-0

Spackman MA, McKinnon JJ (2002) Fingerprinting intermolecular interactions in molecular crystals. CrystEngComm 4(66):378–392. https://doi.org/10.1039/b203191b

Spackman PR, Turner MJ, McKinnon JJ, Wolff SK, Grimwood DJ, Jayatilaka D, Spackman MA (2021) CrystalExplorer: a program for Hirshfeld surface analysis, visualization and quantitative analysis of molecular crystals. J Appl Crystallogr 54(Pt 3):1006–1011. https://doi.org/10.1107/S1600576721002910

Trzesowska-Kruszynska A, Kruszynski R, Zalewicz M, Bartczak TJ (2010) Coordination sphere geometry changes of lanthanoid(III) nitrate complexes with hexamethylenetetramine. J Coord Chem 63(6):1013–1028. https://doi.org/10.1080/00958971003682006

Underwood CC, McMillen CD, Kolis JW (2014) Hydrothermal synthesis and crystal chemistry of novel fluorides with A$_7$B$_6$F$_{31}$ (A = Na, K, NH4, Tl; B = Ce, Th) compositions. J Chem Crystallog 44(10):493–500. https://doi.org/10.1007/s10870-014-0532-4

Westerhausen M (Ed.) (2017) s-Block Metal Complexes (1st ed.) MDPI https://doi.org/10.3390/books978-3-03842-590-8

Whitesides GM, Boncheva M (2002) Beyond molecules: self-assembly of mesoscopic and macroscopic components. Proc Natl Acad Sci 99(8):4769–4774. https://doi.org/10.1073/pnas.082065899

Yao XJ, Xuan YW, Wu W (2008) Hexaaqua-zinc(II) dichloride bis-(hexa-methyl-enetetramine) tetra-hydrate. Acta Crystallog E 64(Pt 9):m1132. https://doi.org/10.1107/S1600536808024793

Yufanyi D, Foba-Tendo J, Ondoh A, Mbadcam J (2014) CdO nanoparticles by thermal decomposition of acadmum-hexamethylenetetramine complex. J Mater Sci Res 3:1–11. https://doi.org/10.5539/jmsr.v3n3p1

Yufanyi D, Ondoh A, Foba-Tendo J, Mbadcam KJ (2015) Effect of decomposition temperature on the crystallinity of α-Fe2O3 (hematite) obtained from an iron(III)-hexamethylenetetramine precursor. Am J Chem 5:1–9

Zhu H-L, Xia D-S, Zeng Q-F, Wang Z-G, Wang D-Q (2003a) Hexaquairon(II) dinitrate bis(dihexamethylenetetramine) tetrahydrate. Acta Crystallog E 59(11):m1020–m1021. https://doi.org/10.1107/s160053680302316x

Zhu H-L, You Z-L, Qu Y, Liu W-S, Tan M-Y, Ma J-L (2003b) Hexaaquanickel(II) dichloride bis(hexamethylenetetramine) tetrahydrate. Acta Crystallog E 59(10):m924–m925. https://doi.org/10.1107/s1600536803020269

Authors and Affiliations

Tambua Neville Milo[1] · Che Dieudonne Tabong[2] · Jean Hubert Nono[3] · Eni Donatus Bekindaka[4] · Divine Mbom Yufanyi[5] · Moise Ondoh Agwara[6]

[1] Department of Chemistry, Faculty of Science, The University of Bamenda, P.O. Box 39, Bambili, Bamenda, Cameroon

[2] Department of Chemistry, Higher Teacher Training College, The University of Bamenda, P.O. Box 39, Bambili, Bamenda, Cameroon

[3] Department of Chemical and Biological Engineering, National Higher Polytechnic Institute, The University of Bamenda, P.O. Box 39, Bambili, Bamenda, Cameroon

[4] Department of Chemistry, Faculty of Science, University of Buea, P.O. Box 63, Buea, Cameroon

[5] Department of Fundamental Science, Higher Technical Teachers' Training College, The University of Bamenda, P.O. Box 39, Bambili, Bamenda, Cameroon

[6] Department of Inorganic Chemistry, Faculty of Science, University of Yaoundé I, P.O. Box 812, Yaoundé, Cameroon